Evolution of the electrode-electrolyte interface of $LiNi_{0.8}Co_{0.15}Al_{0.05}O_2$ electrodes due to electrochemical and thermal stress

Zachary W. Lebens-Higgins,[†] Shawn Sallis,[‡] Nicholas V. Faenza,[¶] Fadwa Badway,[¶] Nathalie Pereira,[¶] David M. Halat,[§] Matthew Wahila,[†] Christoph Schlueter, [||,⊥] Tien-Lin Lee,[||] Wanli Yang,[#] Clare P. Grey,[§] Glenn G. Amatucci,[¶] and Louis F. J. Piper*[,†,‡]

[†]Department of Physics, Applied Physics and Astronomy, Binghamton University, Binghamton, New York 13902, United States

[‡]Materials Science & Engineering, Binghamton University, Binghamton, New York 13902, USA

[¶]Energy Storage Research Group, Department of Materials Science and Engineering, Rutgers University, North Brunswick, New Jersey 08902, United States

[§]Department of Chemistry, University of Cambridge, Lensfield Road, Cambridge, CB2 1EW, U.K.

[||]Diamond Light Source Ltd., Diamond House, Harwell Science and Innovation Campus, Didcot, Oxfordshire OX11 0DE, UK

[⊥]DESY Photon Science, Deutsches Elektronen-Synchrotron, 22603 Hamburg, Germany

[#]Advanced Light Source, Lawrence Berkeley National Laboratory, Berkeley, California 94720, USA

Abstract: For layered oxide cathodes, impedance growth and capacity fade related to reactions at the cathode-electrolyte interface (CEI) are particularly prevalent at high voltage and high temperatures. At a minimum, the CEI layer consists of Li_2CO_3, LiF, reduced (relative to the bulk) metal-ion species, and salt decomposition species but conflicting reports exist regarding their progression during (dis)charging. Utilizing transport measurements in combination with x-ray and nuclear magnetic resonance spectroscopy techniques, we study the evolution of these CEI species as a function of electrochemical and thermal stress for $LiNi_{0.8}Co_{0.15}Al_{0.05}O_2$ (NCA) particle electrodes using a $LiPF_6$ ethylene carbonate: dimethyl carbonate (1:1 volume ratio) electrolyte. Although initial surface metal reduction does correlate with surface Li_2CO_3 and LiF, these species are found to decompose upon charging and are absent above 4.25 V. While there is trace $LiPF_6$ breakdown at room temperature above 4.25 V, thermal aggravation is found to strongly promote salt breakdown and contributes to surface degradation even at lower voltages (4.1 V). An interesting finding of our work was the partial reformation of LiF upon discharge which warrants further consideration for understanding CEI stability during cycling.

INTRODUCTION

The electrode-electrolyte interface (EEI) layer of anodes is well studied in terms of its formation and how it affects battery performance.[1,2] A solid electrolyte interface (SEI) layer forms on the anode surface due to electrolyte reduction reactions and contains various lithium species including LiF, Li_2CO_3 and a series of organics.[3,4] The SEI layer provides a barrier against further electrolyte reduction without significantly hindering Li-ion conduction resulting in high columbic efficiencies after initial formation.[2,3,5] In contrast, the cathode-electrolyte interface (CEI) is less understood regarding its own stability and its role in preventing subsequent electrolyte oxidation reactions.[2]

For layered oxide cathodes, reactions at the CEI are known to contribute to capacity fade and impedance growth particularly when cycling to high voltages (≥4.5 V)[6–9] and at high temperatures.[10,11] The capacity fade and impedance growth arise from a combination of electrolyte decomposition[2,12,13], surface oxygen loss[2,14,15], and transition metal dissolution[6,16] resulting from reactions at the CEI. Highly reactive HF is often linked to the formation of electrolyte decomposition species and active material degradation[17], yet the resulting CEI layer is complicated by the wide range of species that can form from solvent or salt decomposition[16,18,19], and cathode electrolyte reactions.[20,21] Further work is required to disentangle the reaction mechanisms and their impact on cell operation.

In our previous two studies, we employed constant voltage holding of PVDF-free powder $Li_{1-x}Ni_{0.8}Co_{0.15}Al_{0.05}O_2$ (NCA) electrodes to isolate the influence of voltage and temperature on reactions at the CEI.[9,22] This methodology circumvented complications associated with incidental PVDF side reactions[12,23] and with cycling induced micro-grinding.[24] In our first study, we correlated impedance growth with surface oxygen loss for NCA electrodes held ≥4.5 V and at room temperature (RT) when minimal LiF or Li_2CO_3 remained at the cathode surface.[9] By holding electrodes at 60°C, our recent study has revealed how the combination of high temperature and high voltage

severely aggravates reactions at the CEI.[22] For NCA electrodes held at 4.75 V and 60°C, extended holding resulted in a marked increase of P-O-F species, transition metal reduction, and transition metal dissolution. A complex exothermic reaction signifies the initiation of transition metal reduction, subsequent dissolution, and plating at the lithium anode. As a result, the lithium anode potential shifts and subsequently, so does the NCA cathode potential Despite these aggressive electrochemical and thermal conditions, x-ray diffraction (XRD) measurements showed that the bulk of the positive material maintained its initial rhombohedral structure indicating that the active material degradation was largely constrained to the surface.[22]

Here, we examine the evolution of the CEI composition using ex-situ x-ray photoelectron spectroscopy (XPS), x-ray absorption spectroscopy (XAS), and nuclear magnetic resonance (NMR) to correlate temperature and voltage with cathode-electrolyte reactions. We further confirm the limited presence and formation of lithium species at high voltages. From comparing electrodes held at room temperature and 60°C, we highlight the role of thermal aggravation in promoting the formation of P-O-F species and transition metal reduction. Only trace P-O-F species were observed at room temperature, even in the highly delithiated state.

EXPERIMENTAL

Electrode preparation and electrochemical characterization. Dried $LiNi_{0.80}Co_{0.15}Al_{0.05}O_2$ (NAT1050, TODA America) powder was mixed in an argon-filled glove box with 2.5 wt. % carbon black (SuperP, MMM) using a mortar and pestle. To examine the effects of Li_2CO_3, we also prepared NCA powder with increased Li_2CO_3 content by deliberately exposing NCA powder to ambient air for two weeks by resting in a hood with constant air flow.

Powder cells (2032 Hohsen) were assembled using lithium metal (FMC) negative electrode with a combination of glass fiber (Whatman), polyolefin (Celgard) and PVDF-HFP depending on the test temperature, with 1M $LiPF_6$ ethylene carbonate: dimethyl carbonate (EC:DMC) (1:1 volume ratio) electrolyte (BASF). Powder mixture comprised of the NCA powder mixed with carbon black without air exposure unless otherwise indicated. Several electrochemical tests were carried out for half cells as follows:

- Charged to 3.6 V (referred to hereafter as C3.6 V), 4.0 V (C4.0 V), 4.25V (C4.25 V), 4.5 V (C4.5 V), or 4.75 V (C4.75 V) at a constant current of 10 mA/g. All at 24°C
- Charged to 4.75 V at a constant current of 25 mA/g, held for 10 hours at a constant voltage of 4.75 V, and discharged to 2.7 V at a constant current of 5 mA/g with all steps at 60°C. Either pristine NCA powder with air exposure (AE) or no air exposure (No AE) was used.
- Charged to 4.1 V, 4.5 V, or 4.75 V at a constant current of 10 mA/g, held for two weeks at a constant voltage, and discharged to 2.7 V at a constant current of 10 mA/g with all steps at 24°C. The holding step was also performed at 60°C at a constant voltage of 4.1 V and 4.5 V while the charge and discharge steps were at 24°C.
- Charged to 4.75 V at 25 mA/g and held for 10 or 175 hours at a constant voltage of 4.75 V. All at 60°C.

Table 1: Representative electrochemical data for NCA powder electrodes. CV refers to the constant voltage holding step during the electrochemical tests.

Cutoff Voltage (V)	Duration at CV (hrs)	CV temp. (°C)	Charge capacity (mAh/g)	Discharge capacity (mAh/g)
State of Charge				
3.6	-	-	21.1	-
4.0	-	-	162.7	-
4.25	-	-	211.4	-
4.5	-	-	231.1	-
4.75	-	-	261.0	-
AE vs. No AE				
4.75	10	60	286.0	230.8
4.75 (AE)	10	60	288.0	211.9
RT vs. 60°C				
4.1	336	24	232.2	170.1
4.5	336	24	324.0	184.4
4.75	336	24	375.5	215.1
4.1	336	60	257.6	149.2
4.5	336	60	352.4	201.2
4.75	10	60	289.1	-
4.75	175	60	644.5	-

The corresponding charge and discharge capacities for these different electrochemical tests are given in Table 1. Electrochemical curves for the state of charge (SOC) electrodes are shown in figure S1. The significant increase in capacity beyond the theoretical value obtained for electrodes held for 175 hrs at 4.75 V and 60°C within this study was previously reported to be a result of an anodic corrosion reaction.[22]

Electrochemical impedance spectroscopy (EIS) scans were carried out using a Biologic VMP3, in a frequency range of 400 kHz to 15 mHz, with a 20 mV sinusoidal amplitude. All EIS scans were obtained under open circuit conditions, either before or after cycling.

X-ray spectroscopy characterization. For all x-ray spectroscopy measurements, disassembled NCA power electrodes were mounted on conductive tape and transferred using vacuum suitcase set-ups between the glovebox and vacuum chamber to avoid air exposure. The NCA powder electrodes were not washed prior to measurements to retain CEI surface species. XPS measurements were performed using a Phi VersaProbe 5000 system at the Analytical and Diagnostics Laboratory (ADL), Binghamton University. Using the Al K_α monochromated source, the effective probing depth is around 4 nm (from which 95% of the signal originates).[25]

Hard x-ray photoelectron spectroscopy (HAXPES) was conducted at beamline I09 at the Diamond Light Source Ltd. (DLS), UK, using a photon energy of hv≈5940 eV (which will be referred to as 6 keV). HAXPES for this photon energy has an effective probing depth of around 15 nm.[25] The C 1s peak for carbon black was aligned to 284.5 eV to account for charging effects. F 1s, Li 1s, and C 1s core regions were scaled based on normalization of nearest nickel core regions to observe changes in surface species relative to underlying NCA. Peak assignments are based on $LiPF_6$, Li_2CO_3, and LiF reference powders and various literature reports.[16,26–28]

Soft XAS measurements were performed in total electron yield (TEY) mode at beamline I09 at the DLS at the same time as HAXPES measurements. Additionally, XAS measurements in surface-sensitive TEY mode and bulk sensitive total fluorescence yield (TFY) mode were performed at beamline 8.0.1 at the Advanced Light Source (ALS) at the Lawrence Berkeley National Laboratory (LBNL). TEY and TFY measurements are representative of up to 5 nm[7] and 100 nm[29] respectively. Duplicate electrodes have been measured at both beamlines and were highly reproducible. To correlate XPS to HAXPES or XAS, duplicate electrodes with comparable electrochemistry were prepared with electrodes being measured during a similar period. For the O K-edge spectra, photon energies were normalized to a TiO_2 reference and scaled to the background. For the Co L_3-edge and Ni L_3-edge, photon energies were normalized to a Ni-metal reference. The Co L_3-edge and Ni L_3-edge spectra were scaled to the peaks at ~780 eV and ~855 eV respectively.

Nuclear magnetic resonance (NMR) characterization. Solid-state ^{19}F magic-angle spinning (MAS) NMR measurements were carried out on a 11.7 T Bruker Avance III 500 MHz spectrometer using a Bruker 1.3 mm HX probe. Experiments were performed under a MAS frequency of 45 or 60 kHz using a rotor-synchronized Hahn echo pulse sequence of the form $(\pi/2)_x$-τ-$(\pi)_y$-τ-acquire with a pulse length of 1.4 μs (optimized $\pi/2$ pulse length for solid AlF_3) and a recycle delay of 250 ms. Spectra were referenced to PTFE at -123 ppm, and were processed with Bruker TopSpin 3.2.

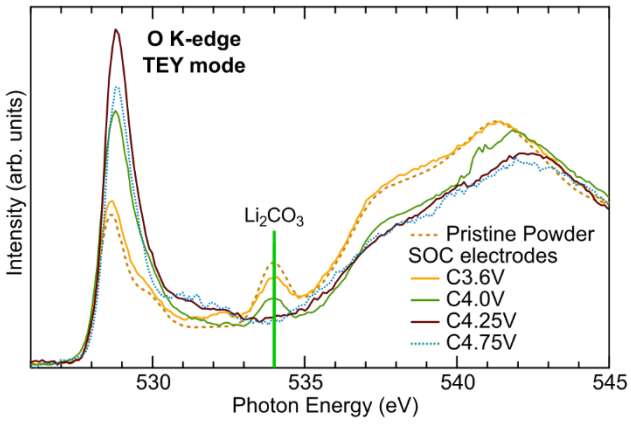

Figure 1. High resolution TEY mode XAS of the O K-edge for pristine NCA powder and SOC electrodes charged to 3.6 V, 4.0 V, 4.25 V, and 4.75 V at RT.

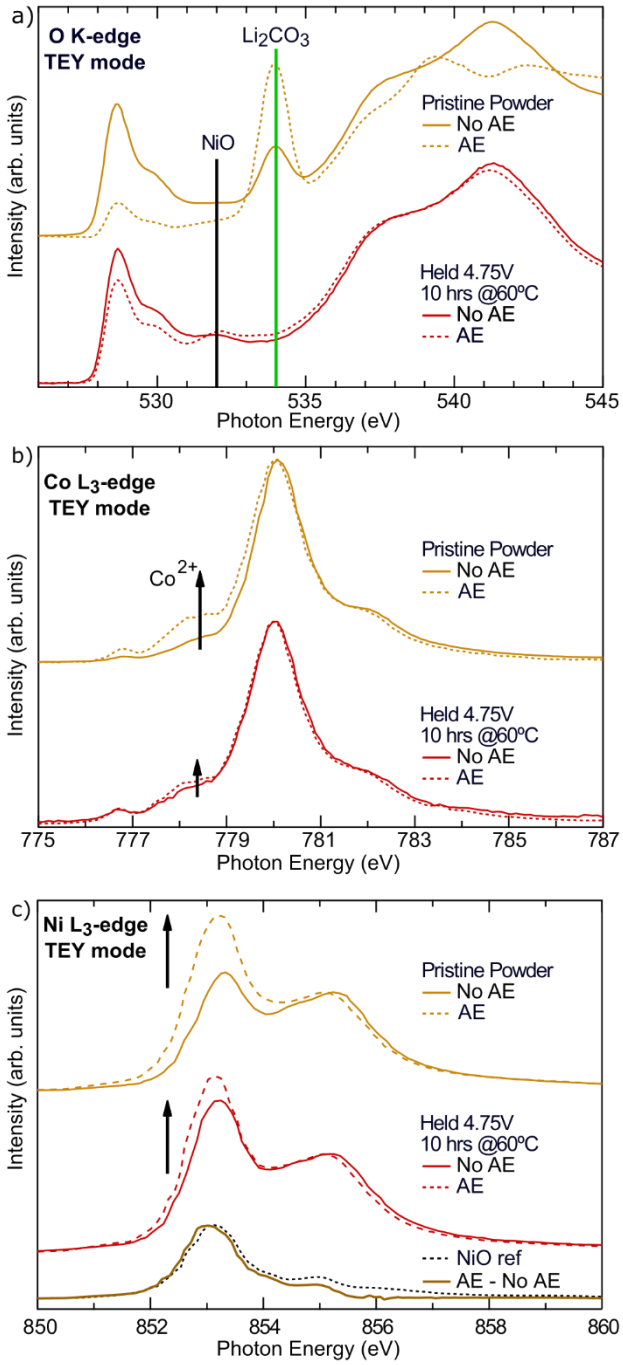

Figure 2. High resolution XAS measurements of the (a) O K-edge, (b) Co L_3-edge, and (b) Ni L_3-edge for electrodes held for 10 hours at 4.75 V and at 60°C, measured in the discharged state (D2.7 V), that used AE and no AE powder and AE and no AE powders. A difference spectrum for the Ni L_3-edge of the powders is included along with a NiO reference.

RESULTS

Breakdown of Li_2CO_3 at the CEI. By measuring the O K-edge for SOC electrodes, we determined that the native Li_2CO_3 layer is lost during the first charge as shown in Fig. 1. In the O K-edge, the peak at 528.7 eV is associated with $Ni^{3+/4+}$-O 2p hybridized states.[30] Peaks at 532 eV and 534 eV are indicators of the formation of NiO-like environments and Li_2CO_3[31], respectively.

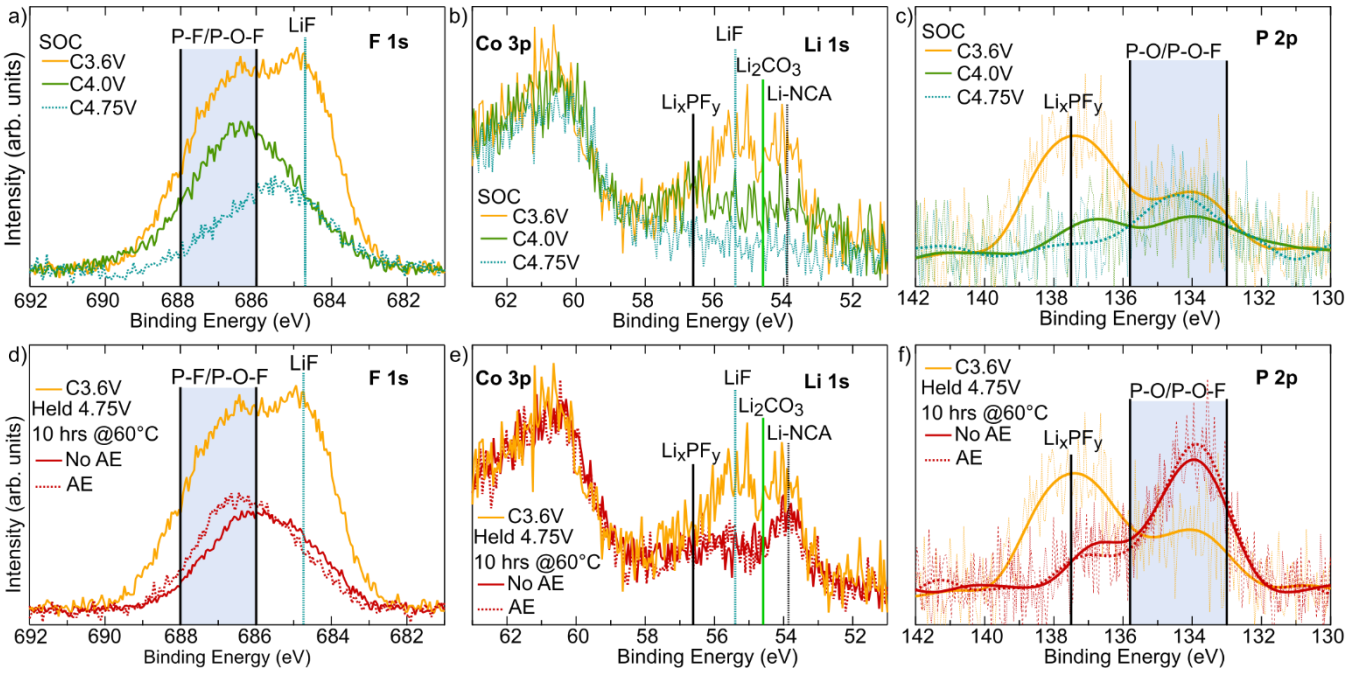

Figure 3. XPS measurements of the F 1s, Li 1s and P 2p core region for (a-c) SOC electrodes and (d-f) electrodes held 10 hrs at 4.75 V and 60°C measured after discharge to 2.7 V. For the electrodes held at 4.75 V and 60°C, NCA powder with AE and no AE were used for the electrodes. The SOC electrodes used pristine powder with no air exposure

Comparing the pristine powder to the C3.6 V electrode, there is a decrease of the Li_2CO_3 peak from initial contact with the electrolyte. Upon further charging, the Li_2CO_3 peak is fully lost between 4.0 V and 4.25 V and is absent at higher voltages. Our results are consistent with a synchrotron XRD study which showed the loss of Li_2CO_3 during the first charge of NCA.[32]

As only a thin Li_2CO_3 overlayer is present on the pristine powder, due to the care taken in avoiding atmospheric exposure, we also prepared electrodes using air exposed NCA powder to examine the effect of a thicker Li_2CO_3 overlayer on the active material. O K-edge measurements for no AE and AE powder are shown in Fig. 2a. The AE process resulted in a roughly 7-fold increase in the Li_2CO_3 content of the initial NCA material evaluated in this study based on previously reported thermogravimetric analysis.[22] For electrodes held for 10 hrs at 4.75 V and 60°C using AE and no AE NCA powder and discharged to 2.7 V, the peak at 534 eV associated with Li_2CO_3 is absent. Therefore, surface Li_2CO_3 decomposes during the first cycle, even when a thicker initial overlayer is present. XPS measurements of duplicate electrodes further confirm the loss of Li_2CO_3 after the first cycle as shown in Fig. S2.

From the corresponding XAS measurements of the Ni L_3-edge and Co L_3-edge for these samples, shown in Fig. 2, we correlated initial Li_2CO_3 formation with increased surface transition metal reduction. For the no AE powder, the Ni L_3-edge and Co L_3-edge lineshapes are representative of Ni^{3+} and Co^{3+} respectively. A NiO reference is included in Fig. 2c as a representative of the high spin Ni^{2+} lineshape, similar to that reported for $LiNi_{0.4}Mn_{0.4}Co_{0.18}Ti_{0.02}O_2$ (NMC)[7] and Ni-Fe-OH complex hydroxide[33]. For the Ni L_3-edge, the Ni^{2+} lineshape has a distinctive lineshape compared to the NCA Ni^{3+} lineshape. Therefore, the increased intensity of the peak between 852 to 854 eV for the AE NCA powder compared to the no AE NCA powder indicates nickel is reduced as a result of the ambient exposure. To confirm reduced Ni^{2+} surface species, we plot the difference spectra, between the Ni L_3-edge for the AE and no AE powder which produces the same lineshape as the NiO reference.

Surface nickel reduction agrees with a previous report that it occurs upon ambient exposure for layered oxide cathodes.[34] We note that various Ni^{2+} compounds could be responsible for the change in the Ni L_3-edge lineshape at the CEI. A recent report identified that H^+/Li^+ cation exchange reactions promote the formation of Li_2CO_3 and similar surface species upon humid air exposure of $LiNi_{0.5}Mn_{0.3}Co_{0.2}O_2$[34]. Scanning transmission electron microscopy measurements identified the formation of a cubic surface phase after extended humid air exposure that was assigned as a $H_{2x}M_{1-x}O$ material[34] which would correspond to the formation of a nickel (II) hydroxide chemical environment. The Co L_3-edge also shows increased Co^{2+} at the surface after AE when comparing the AE powder to the no AE powder. Moreover, after the decomposition of the Li_2CO_3 layers, the electrode held for 10 hrs at 4.75 V and 60°C using AE powder has more nickel reduction than the corresponding electrode using no AE powder.

Loss of lithium species from the CEI layer at high voltages. From XPS measurements, we identified changes in the electrolyte decomposition species at the CEI during the first charge. The F 1s, P 2p, and Li 1s core regions for C3.6 V, C4.0 V and C4.75 V electrodes are shown in Fig. 3a-c. For the C3.6 V electrode, we identified the surface species that form upon initial contact with the electrolyte. Based on the peaks at 684.8 eV and 55.4 eV in the F 1s and Li 1s core regions respectively, LiF is present on the surface of the

NCA particles likely due to reactions induced by the $LiPF_6$ electrolyte or residual HF in the electrolyte which includes some breakdown of the initial Li_2CO_3 layer.[35] The additional peak present in the F 1s core region at 687 eV is assigned as Li_xPF_y[12]/$LiPF_6$ species with a corresponding peak at 137.5 eV in the P 2p core region. As electrodes are charged to higher voltages, there is a large decrease in the F 1s intensity due to the loss of LiF and Li_xPF_y from the surface. In the P 2p core region, there is a loss of the Li_xPF_y peak and a weak peak that remains at 134 eV, attributed to a surface P-O or P-O-F species.[16] At 4.75 V, Li 1s peaks are below the detection limit due to the loss of lithium surface species and the removal of lithium from the active material. Although there is a large decrease in the F 1s intensity at high states of charge, some fluorine species remain on the surface at 4.75 V which may include a mix of P-O-F and residual LiF species.

XPS measurements of electrodes held for 10 hrs at 4.75 V and 60°C using no AE and AE powder were performed to determine the influence of Li_2CO_3 on reactions at the CEI. The F 1s, P 2p and Li 1s core regions for these electrodes are compared with a C3.6 V electrode, as shown in Fig. 3. Comparing the C3.6 V sample and electrodes held 10 hrs at 4.75 V, there is a decrease in the peaks associated with LiF. Additionally, we do not observe a Li_xPF_y peak for the held electrodes in the P 2p core region but do observe an increased formation of a P-O/P-O-F species due to holding at 4.75 and 60°C. Overall, the 4.75 V 10 hrs electrodes have a similar composition of $LiPF_6$ decomposition species at the surface, with the electrode using AE powder having only slightly more fluorine and phosphorous surface species, despite the presence of a much thicker initial Li_2CO_3 overlayer. Under these electrochemical conditions, the Li_2CO_3 breakdown does not seem to have a pronounced effect on the electrolyte decomposition species at the CEI.

Influence of temperature on $LiPF_6$ decomposition species at CEI. To examine the influence of temperature and voltage on electrolyte decomposition species and transition metal reduction, electrodes were held for two weeks at a constant voltage of 4.1 V, 4.5 V, or 4.75 V and at either RT or 60°C and subsequently discharged to 2.7 V. All subsequent electrochemical studies discussed used pristine powder with care taken to minimize Li_2CO_3 formation. Previously reported XAS measurements of the O K-edge and Ni L-edge for electrodes held for two weeks at 4.1 V, 4.5 V, and 4.75 V and at RT and discharged to 2.7 V showed increased nickel reduction when holding at ≥4.5 V that correlated with positive electrode impedance growth.[9] The electrode held at 4.1 V and RT was shown to have a comparable Ni L-edge lineshape as the reference C3.6 V electrode since minimal surface reduction occurs under these conditions.[9] Here, we compare XAS measurements for duplicate cells to compare room temperature and 60°C holding.

Comparison of the O K-edge and Ni L_3-edge in TEY mode for electrodes held for two weeks at RT and 60°C are shown in Fig. 4. From examination of the O K-edge, there are no clear peaks associated with Li_2CO_3 for the electrodes held at 4.1 V or 4.5 V. Therefore, Li_2CO_3 is not readily formed electrochemically when holding at

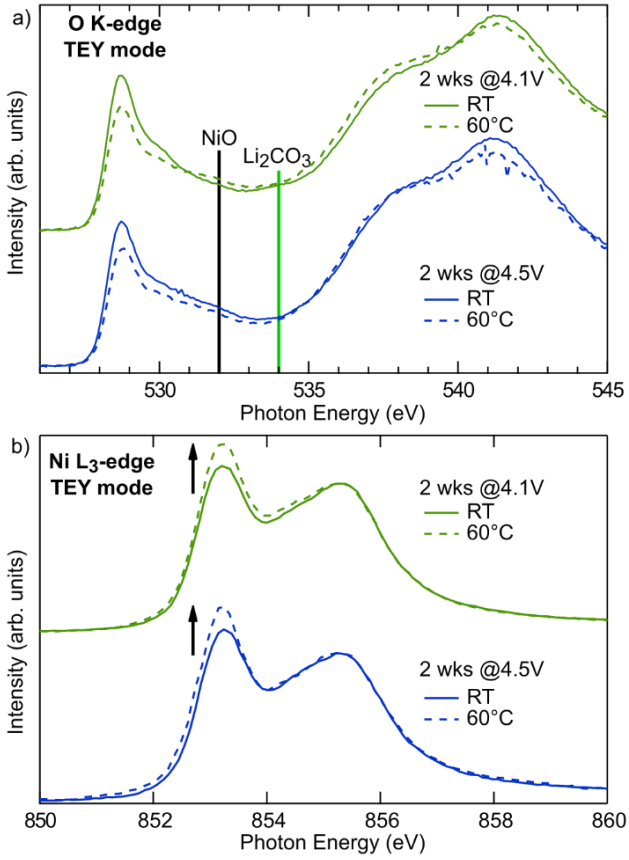

Figure 4. XAS measurements of the a) O K-edge and b) Ni L_3-edge in TEY mode for electrodes that were held for two weeks at 4.1 V and 4.5 V at either RT or 60°C and discharged to 2.7 V.

voltages ≥4.1 V and does not necessarily reform on the surface during discharge. At higher temperatures, there is a decrease in the pre-edge peak at 528.7 eV either because of surface oxygen loss or the formation of surface oxygen species that decrease the signal from the active material. Increased intensity in the Ni L_3-edge at 853 eV indicates Ni^{2+} formation at higher temperatures, even when holding at 4.1 V. This is consistent with an electron energy loss spectroscopy study that showed increased surface oxygen loss when cycling to 4.3 V at 55°C compared to room temperature cycling.[15] As there are minimal lineshape changes of the O K-edge and Ni L_3-edge in TFY mode, shown in Fig. S3, the transition metal reduction is limited to the first few nm. Co L_3-edge measurements of the held electrodes, shown in Fig. S4, indicate that appreciable cobalt surface reduction occurs only when holding at higher voltages and 60°C.

XPS measurements of the F 1s, Li 1s and P 2p core regions for electrodes held for two weeks at either RT or 60°C, shown in Fig. 5, were examined to correlate electrolyte decomposition with transition metal reduction. A C3.6 V reference is included for comparison that was measured as part of the two week held set. In contrast to the high SOC electrodes where peaks in the Li 1s associated with surface species are below observable levels, peaks between 54.5 eV and 58 eV are present after discharge.

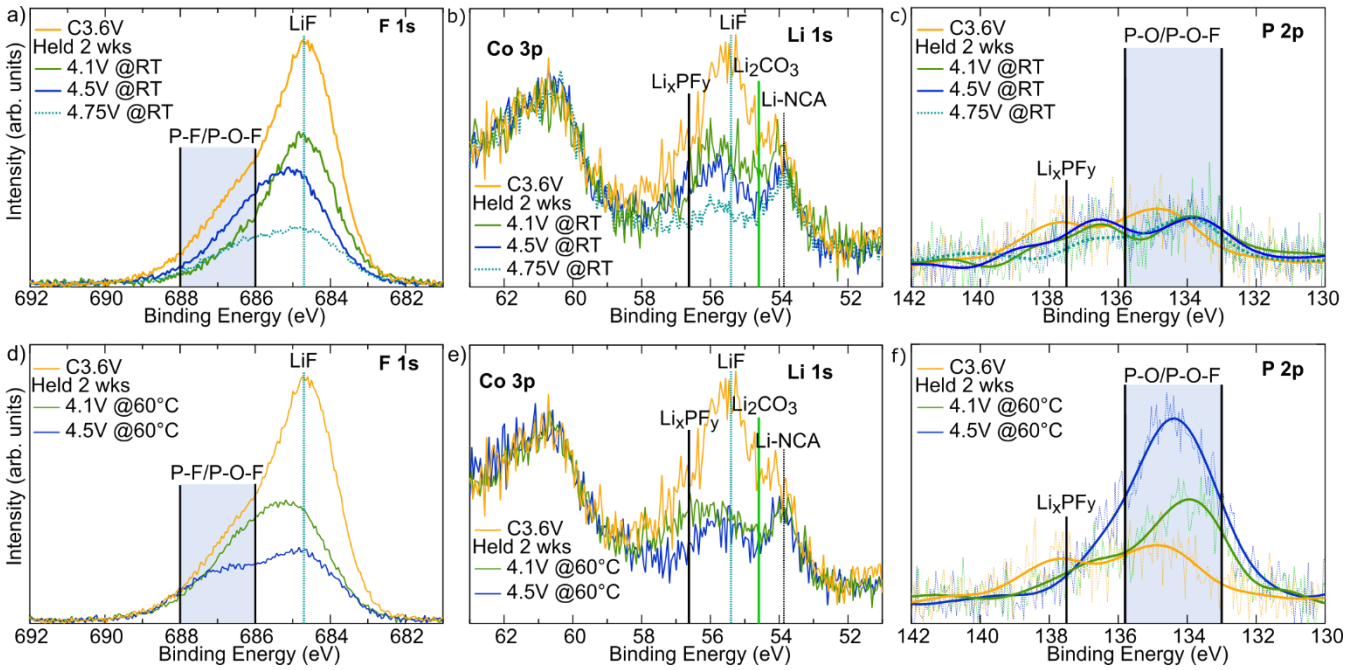

Figure 5. XPS measurements of the F 1s, Li 1s, and P 2p core regions for electrodes held at (a-c) RT or at (d-e) 60°C for two weeks. All electrodes were measured in the discharged state (D2.7 V) and an electrode charged to 3.6 V is included for reference.

The presence of the Li 1s surface peak around 55.4 eV indicates that LiF is reformed during the discharge. For the electrodes held at RT, the Li 1s and F 1s peaks associated with LiF decrease in intensity for electrodes held at higher voltages with the electrode held at 4.75 V having the lowest intensity. We also observed the decrease of other higher binding energy Li 1s peaks above 56.6 eV when holding at higher voltages which includes the loss of Li_xPF_y. Based on the minimal changes in the P 2p peaks for the electrodes held at 4.1 V, 4.5 V and 4.75 V, there is limited formation of phosphorous species as a result of holding at RT. Although nickel reduction increases when holding at ≥4.5 V and RT, there is no clear concurrent growth of electrolyte decomposition species. Holding at 4.5 V and 4.75 V for four weeks instead of two weeks revealed only a trace increase in surface species which are primarily identified as P-O-F and C-H species as shown in Fig. S5.

In contrast to holding at RT, electrodes held at 60°C have a pronounced increase in P-O-F surface species particularly at higher voltages. For the electrodes held for two weeks at 4.1 V and 4.5 V and at 60°C, there is an increase of the P 2p core region peak that is centered between a binding energy of 133 eV and 135 eV which grows with holding at higher voltages. The peak position is consistent with the formation of P-O-F surface species based on previous XPS studies.[16,26] Although higher energy peaks in the F 1s core region between 686 eV and 688 eV cannot be assigned with certainty to a specific species due to the similar peak positions for different P-O-F and Li_xPF_y species[26], intensity differences between electrodes held at RT and 60°C are consistent with the formation of P-O-F species. Despite the increased $LiPF_6$ decomposition species from holding at 60°C, there is a similar loss of surface lithium species as was observed for RT holding. While LiF reforms at the cathode surface during discharge, the quantity of LiF present after discharge is dependent on the temperature and voltage at which the electrodes are held.

Table 2. Diameter of the first semi-circle associated with the negative electrode impedance based on EIS measurements before charge and after discharge for electrodes that are held at 2 weeks at either 4.1 V, 4.5 V, or 4.75 V and room temperature or 60°C.

Cutoff Voltage (V)	Initial Impedance (Ω)	Final Impedance (Ω)
4.1 @RT	272.93	264.40
4.5 @RT	193.46	225.02
4.75 @RT	248.18	246.43
4.1 @60C	224.69	222.19
4.5 @60C	192.44	659.15

The listed impedance values in Table 2 are a measure of the diameter (magnitude) of the first semi-circle which is correlated to the impedance of the negative electrode. This is based on previously reported three-electrode measurements.[22] The second semi-circle, which is generally associated with the positive electrode, is only partially visible for all tests because the cells were measured in the fully lithiated state. Nyquist plots for these electrodes are shown in Fig. S6. As a result, the listed impedance of the first semi-circle is a measure of the impedance of the entire cell, but the growth in this impedance can't be conclusively tied to the CEI formation. However, only the combination of high temperature and high voltage impacted impedance that lead to a 3-fold increase in the charge transfer impedance after 2 weeks at 4.5 V and 60°C.

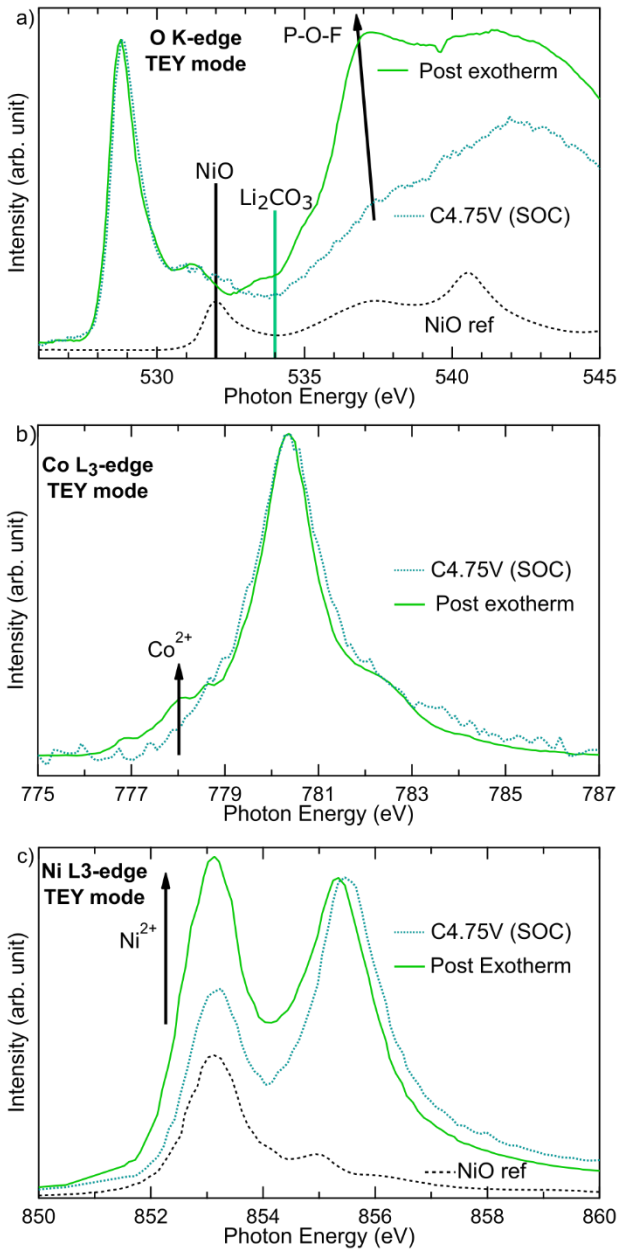

Figure 6. High resolution XAS comparing the (a) O K-edge, (b) Co L3-edge, and (c) Ni L3- edge for the post exotherm electrode compared with a C4.75 V at RT electrode. Both electrodes are measured highly delithiated at SOC. The O K-edge is scaled to the main NCA peak at 528.8 eV.

Since there was no impedance development on the 4.1 V and 60°C sample, the large impedance increase on the 4.5 V and 60°C sample is not solely due to the elevated temperature. Because the lithium negative electrode is independent of the cell's SOC, the impedance rise of the 4.5 V and 60°C sample must be correlated to either the positive electrode or electrolyte. Thus, the impedance development is either associated to poisoning of the negative electrode by the dissolution of transition metal ions from the positive electrode or from the degradation of the electrolyte, which has already been shown to form P-O-F species on the positive electrode.

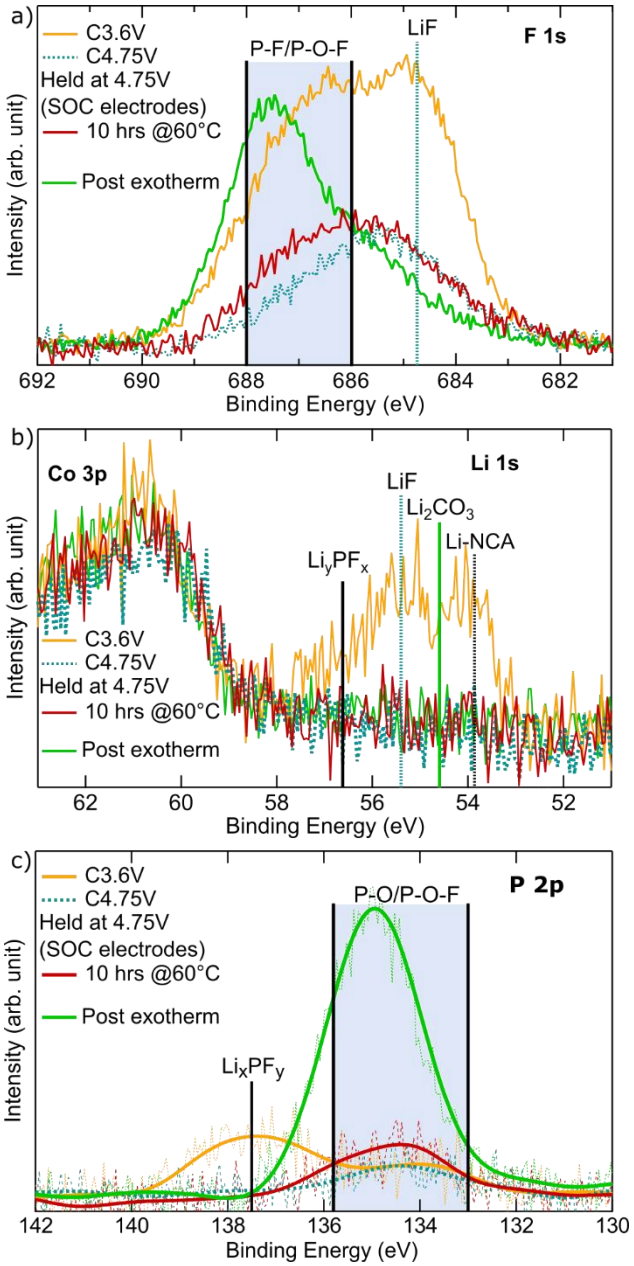

Figure 7. (a) F 1s, (b) Li 1s, and (b) P 2p core regions for the electrode held for 10 hours at 4.75 V and 60°C and the post exotherm electrode measured in the highly delithiated state. A C3.6 V and C4.75 V SOC electrodes that were charged at RT are shown for comparison

Enhanced $LiPF_6$ decomposition under extreme electrochemical and thermal stress. When layered oxide cathodes are held at 4.75 V and 60°C for an extended period, the combined electrochemical and thermal stress results in a complex exothermic reaction signifying the initiation of transition metal reduction, subsequent dissolution and plating at the lithium anode which is followed by the shift of the lithium anode potential and subsequently the NCA cathode potential.[22] While a thorough study of the exothermic reaction and the influence of cathode degradation is reported separately[22],

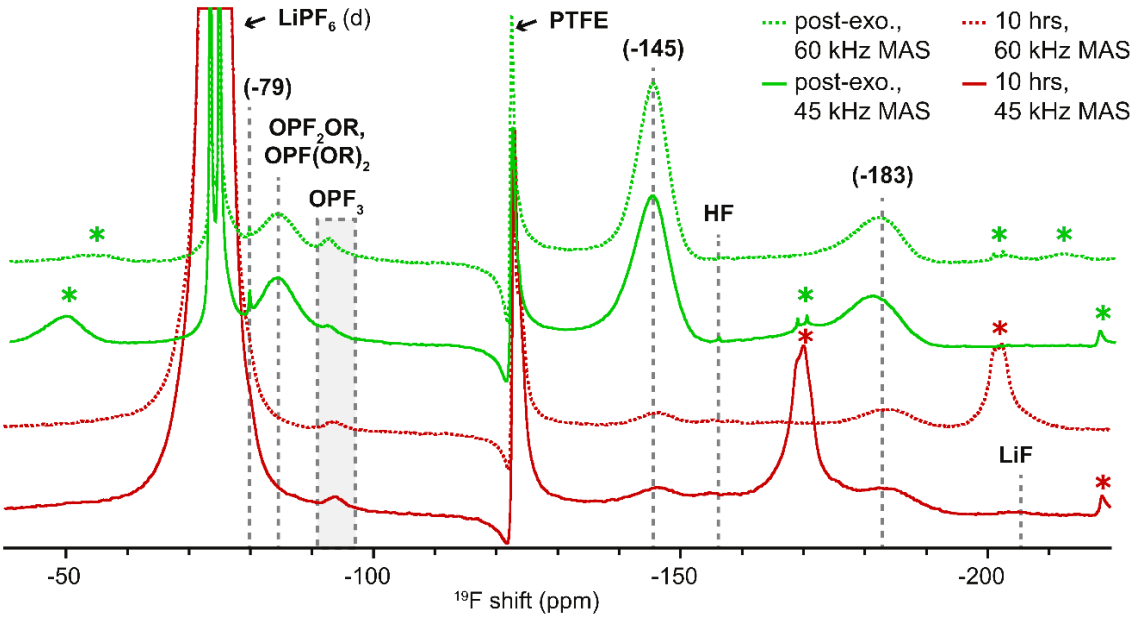

Figure 8. ^{19}F MAS NMR spectra of the post-exotherm electrode and the electrode held at 10 hrs and measured in the highly delithiated state shows features assigned to predominantly P-O-F decomposition species between -85 and -95 ppm. The feature at -123 ppm arises from PTFE tape packed into the MAS rotor to aid in spinning the limited quantity of sample. Spectra have been acquired at 11.7T at a MAS rate of 45 and 60 kHz. Asterisks denote spinning sidebands.

we provide further insight into the electrolyte decomposition species that form under these extreme conditions and compare with the species that form under more moderate conditions. The large growth of impedance at the lithium anode, due to transition metal plating and electrolyte reduction reactions, prevents discharge of the cathode. Therefore, NCA electrodes held for 175 hrs at 4.75 V vs V_{neg} and 60°C, which will be referred to as post exotherm electrodes, are primarily compared to a C4.75 V SOC electrode as the same bulk nickel and cobalt oxidation states are expected for these electrodes due to similar levels of bulk delithiation.

While XAS measurements of post-exotherm electrodes are previously reported, here we present higher resolution XAS measurements performed at the DLS that allow for identification of additional spectral features. XAS measurements of the O K-edge, Co L_3-edge, and Ni L_3-edge for the C4.75 V and the post-exotherm electrodes are shown in Fig. 6. In the O K-edge, there is a more distinct feature at 535 eV and a large increase in intensity between 536-538 eV that was not observed for other held electrodes. For various phosphorus oxide compounds, including $LiPO_3$, $Li_4P_2O_7$, and Li_3PO_4, similar features are present at these photon energies related to P-O hybridized unoccupied states.[36] From the Ni L_3-edge and Co L_3-edge, holding for 175 hrs at 4.75 V and 60°C resulted in an increase in transition metal reduction compared to the C4.75 V electrode. In particular, there is a much larger change in the Ni L_3-edge lineshape than for any of the electrodes held for two weeks at lower voltages or at RT. Active material degradation is more pronounced than can be observed with just the Ni L_3-edge and Co L_3-edge measurements as a large increase in transition metal dissolution occurs under these aggressive conditions.[22] Previously reported XRD and partial fluorescence yield measurements confirm the reduction is confined to the surface.[22]

From XPS measurements of the F 1s, Li 1s, and P 2p core regions shown in Fig. 7, holding at 4.75 V and 60°C results in extensive P-O-F species and no observed lithium species formation. Holding for 175 hours at 4.75 V and 60°C resulted in the growth of a higher energy peak at 687.6 eV in the F 1s core region and a corresponding increase in the P 2p peak at 135 eV. The F 1s peak and P 2p core region peak positions are consistent with previously reported P-O-F species[16,26] Moreover, features in the O K-edge assigned as P-O hybridized states are consistent with the growth of P-O-F surface species. While intensity increases of P-O-F features are markedly higher than when holding for two weeks at lower voltages at 60°C, the similar P 2p peak positions indicate similar species formation at these lower voltages.

To confirm the presence and identity of the P-O-F species, ^{19}F MAS NMR experiments were performed on electrodes held (1) for 10 hours and (2) for 175 hours at 4.75 V and 60°C. These measurements are challenging due to the paramagnetic behavior of the NCA electrodes that leads to shortened spin-lattice (T_1) and spin-spin (T_2) relaxation times; nonetheless, we have successfully acquired ^{19}F NMR spectra at 11.7 T and a MAS rate of 45 or 60 kHz (Fig. 8). As Campion et al. have reported[37], the solution-state ^{19}F NMR shifts of various OPF_2OR and $OPF(OR)_2$ species (R = Me, Et) lie between -83.5 and -88.3 ppm.[38] In the sample held for 175 hours, we therefore assign the broad feature at -85 ppm to these P-O-F decomposition products in the disordered CEI. A $LiPF_6$ component at -74.5 ppm (doublet) is also observed in both samples, with the doublet arising from scalar coupling to ^{31}P (I = ½).

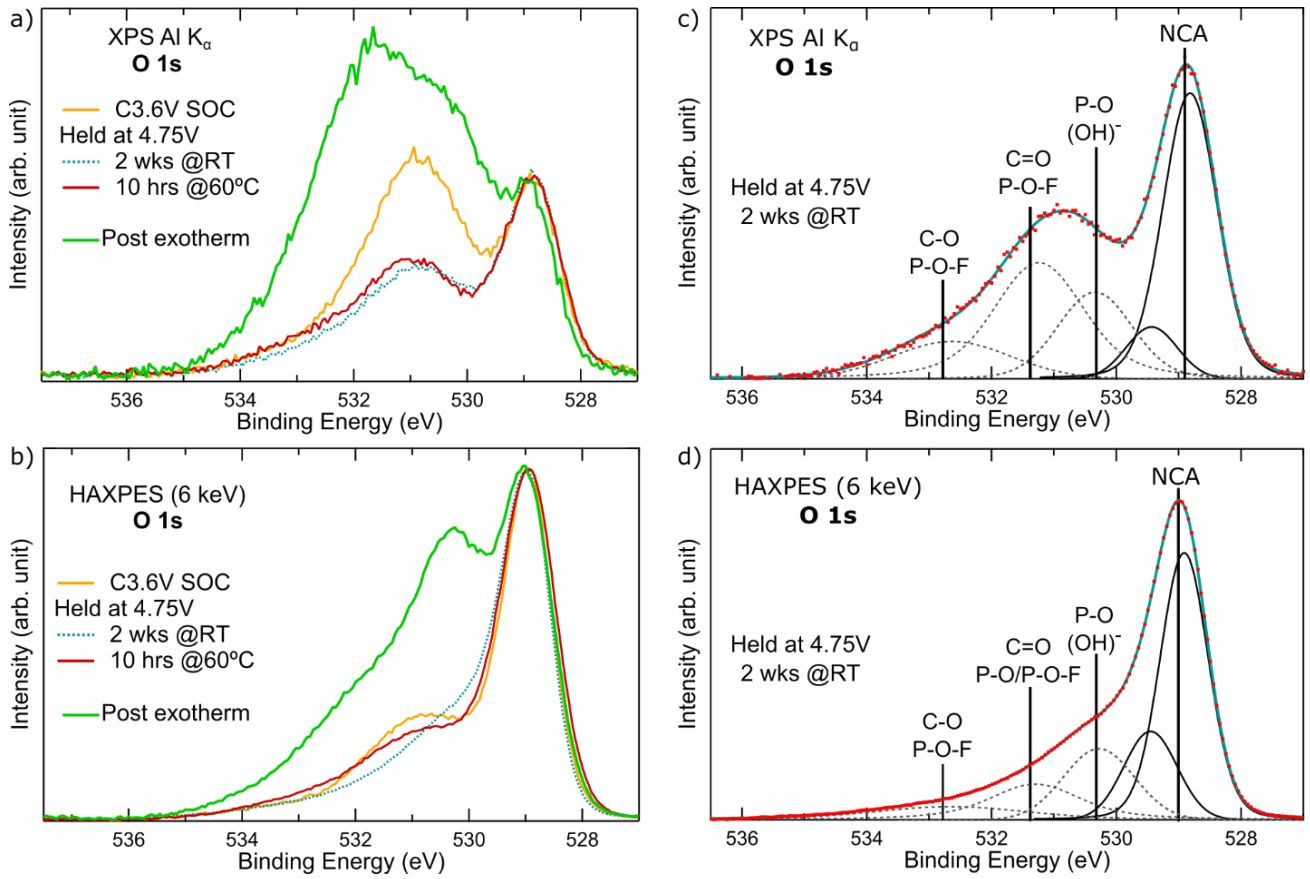

Figure 9. O 1s core region at (a) 1484.6 eV and (b) 6 keV for electrodes held at 4.75 V for 2 weeks at RT and for 10 hours at 60°C, measured after discharge to 2.7 V, and the post exotherm (175 hrs at 60°) electrode, measured in the highly delithiated state, and compared with a C3.6 V SOC reference scaled to the lattice oxygen peak at 529 eV. Peak fits of the O 1s core region measured with (c) XPS and (d) HAXPES for the electrode held for 2 weeks at 4.75 V and RT and discharged to 2.7 V, which was selected as a representative example. Peaks associated with the NCA bulk and surface species are identified with solid lines and dotted lines respectively

The sharpness of this feature indicates that the $LiPF_6$ resides in a solution-like or semi-solid phase (e. g., still trapped on the electrode surface). Minimal intensity arising from organic decomposition products is seen in the sample held at 10 hours, in excellent agreement with the F 1s and P 2p XPS data (Fig. 7a), confirming that the exothermic reaction leads to a noticeable increase in the quantity of P-O-F species. A feature at roughly -93 ppm is observed in both samples which is tentatively assigned to a minor OPF_3 component.[37] A weak LiF signal at -205 ppm appears only in the sample held for 10 hours, suggesting that the concentration of this phase decreases following the exothermic reaction. Finally, the isotropic ^{19}F shifts at -145, -159 and -183 ppm appear consistently across a wide range of cycled electrodes, and are assigned to inorganic components including species containing aluminum that presumably originate from aluminum within the electrode. This assignment will be addressed in a separate study focusing on the surface aluminum environments.

Further examination of the O 1s core region, as shown in Fig. 9 for select electrodes held at 4.75 V and a C3.6 V electrode, allowed for quantifying surface species that formed during constant voltage holding. The electrodes held for 10 hrs and for two weeks are measured in the discharged state (D2.7 V). Based on the intensity increase of higher binding energy features in XPS compared to HAXPES that has higher bulk sensitivity, we identified these features as surface environments.

HAXPES and XPS peak fits of the O 1s core region for the electrode held at 4.75 V and RT for two weeks are shown in Fig. 9(c-d). Two peaks were used to fit the asymmetry of the main O 1s peak at 529.0 eV associated with lattice oxygen. Higher energy peaks at 530.2 eV, 531.2 eV, and 532.6 eV are roughly assigned as surface hydroxides[39], O-C=O/P-O-F[26,28], and CO/P-O-F.[26,27] For the C3.6 V electrode, the main surface peak at 531.0 eV is assigned as Li_2CO_3 based on the Li_2CO_3 peak observed in the O K-edge shown in Fig. 1. Peak assignments account for the C 1s peak position used for calibration and separations between the O 1s lattice peak and surface peaks within these studies. Various P-O and P-O-F species likely contribute to the surface O 1s peaks between 531 to 534 eV particularly for the post-exotherm electrode that has a broad O 1s surface peak where additional peaks were needed to fit the O 1s lineshape.

While some of the oxygen surface species may be assigned to C-O/C=O species, there are minimal changes in the C 1s core region, shown in Fig. 10, as a result of constant voltage holding. The C 1s core region was scaled based on normalization of the Ni 3p core region. Variation of the intensity of the main carbon black peak is related to the changes in the surface species composition that can attenuate the signal from the active material.

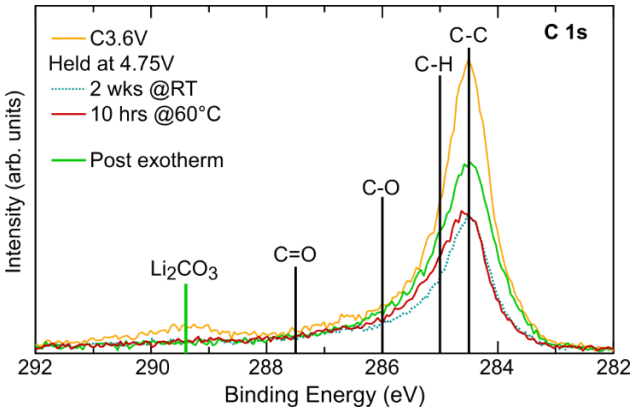

Figure 10. XPS measurements of the C 1s core region for a C3.6 V electrode and select electrodes held at 4.75 V. The electrodes held for 4.75 V for 2 weeks at RT and 10 hours at 60°C are measured after discharge to 2.7 V while the post exotherm electrode is measured in the delithiated state

Cycling studies have observed formation of C-H, C-O and C=O species that are assigned at 285 eV, 286.0 eV, and 287.5 eV, respectively.[16,26,27] As electrodes contain no PVDF and only 2.5 wt. % carbon black, which is lower than reported for other studies[26,27,40,41], clear changes in the C 1s peak relative to the carbon black peak at 284.5 eV would be expected from the formation of solvent decomposition species. While we observed some change in the C 1s lineshape that may be related to C-H formation, there are limited changes at higher binding energy (≥285.5 eV) that would correspond to C-O and C=O solvent decomposition species. Therefore, the growth of oxygen surface species at the CEI is mainly associated with the formation of P-O and P-O-F from $LiPF_6$ decomposition rather than the formation of C-O or C=O from solvent decomposition.

Considering the probing depth of HAXPES and XPS, the portion of the CEI layer consisting of electrolyte decomposition species is likely <5 nm for all samples (evenpost-exotherm). This agrees with the TEY measurements of the O K-edge for which peaks associated with the active material are clearly distinguishable for all electrochemical testing conditions. This thickness is comparable to the spatial extent of the reduced Ni surface layer of the CEI i.e. < 10 nms of the NCA particle surface

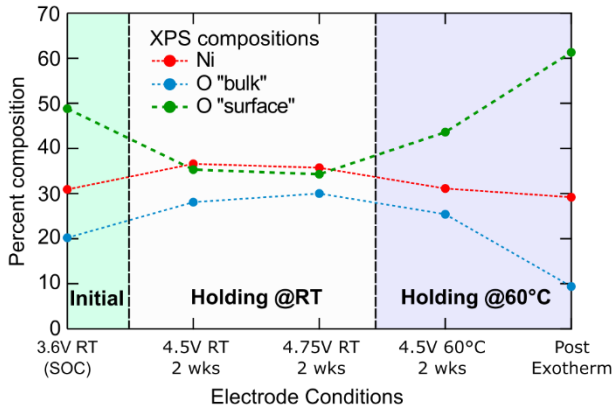

Figure 11. Comparison of oxygen "bulk", oxygen "surface" and nickel composition for held electrodes determined from the peak fits of the O 1s and Ni 2p core region measured at 1486.6 eV.

based on previous high-resolution transmission electron microscopy measurements.[9,22]

To illustrate the variation in the electrolyte decomposition layer thickness, a comparison of the Ni, O "bulk", and O "surface" compositions are shown in Fig. 11 based on XPS peak fits for select electrodes held at RT or 60°C. The oxygen "bulk" percentage is based on the area of the two peaks used to fit the main NCA peak while the oxygen "surface" percentage is based on the area of peaks between 530 to 534 eV.

Additional peak fits of the O K-edge, Li 1s, and P 2p were used to quantify the changes in the surface Li_2CO_3, lithium species, and P-O-F species respectively as shown in Fig. 12. Representative spectra and peak fit components are shown in Fig. S7. The Li_2CO_3 is based on the O K-edge peak at 534 eV (Fig. 1) and scaling of the O K-edge to the background. We note that there is no longer a clear Li_2CO_3 peak in the O K-edge for the electrodes charged above 4.0 V and all the held electrodes. The surface Li 1s species are based on peaks from 54.5 eV to 58 eV (Fig. 3). The P-O-F peaks are based on peak area in P 2p core region from 133.5 eV to 135.5 eV. (Fig. 3)

DISCUSSION

From our characterization of NCA powders and held electrodes, we identify three distinct regimes of the CEI layer composition: initial lithiated state, delithiated state at RT, and delithiated state at 60°C as illustrated in Fig. 11. The initial CEI layer, after exposure to the electrolyte, was observed to mainly consist of lithium species including Li_2CO_3 and LiF. During the first charge LiF and Li_2CO_3 are lost from the surface with minimal lithium species present at high voltages, as shown in Fig. 12b. Li_2CO_3 was previously observed to decompose in the $LiPF_6$ electrolyte from reactions with $LiPF_6$ or residual HF; although electrochemical stress may induce a more rapid decomposition. The decomposition of Li_2CO_3 upon reactions with $LiPF_6$ or residual HF can result in the formation of LiF, POF_3, and CO_2.[35,42,43]

$$LiPF_6 + Li_2CO_3 \rightarrow POF_3 + CO_2 + 3\,LiF \quad (1)$$

$$2HF + Li_2CO_3 \rightarrow 2LiF + CO_2 + H_2O \quad (2)$$

Although Li_2CO_3 has been reported to decompose and reform during the first few cycles resulting in sluggish kinetics for NCA electrodes[32], minimal surface Li_2CO_3 reformation is observed after electrodes held at ≥4.1 V are discharged to 2.7 V as shown in Fig. 12a. A recent report has identified the initial thickness of Li_2CO_3 and the role of this initial layer on the reaction heterogeneity of the NCA material during the first charge.[44]

When holdings at high voltages at RT, there is minimal evidence of buildup of electrolyte decomposition species at the CEI despite the growth of a disordered spinel phase due to surface oxygen loss at ≥4.5 V.[9] In addition to the absence of significant LiF and Li_2CO_3 at the surface, there is minimal formation of $LiPF_6$ decomposition species even when holding at 4.75 V. This suggests that the $LiPF_6$ is relatively stable at these high voltages at RT though we cannot account for changes in the concentration of soluble decomposition species in the electrolyte.

In contrast, thermal aggravation at high voltages does lead to pronounced $LiPF_6$ decomposition. At high voltages and high temperatures, we observed bone-fide $LiPF_6$ decomposition leading to the formation of P-O-F species as shown in Fig. 12c. Furthermore, holding at 60°C led to more P-O-F species at 4.1 V than were present at high voltages at RT. NMR measurements of $LiPF_6$ salt in DEC, DMC, and EC solutions reported predominately HF and P-O-F species formation from reactions with protic impurities in the electrolyte as a result of thermal decomposition of the $LiPF_6$ salt.[37] Here, cathode electrolyte reactions are enhanced at high voltages by the thermal decomposition of the $LiPF_6$ salt. This results in increased surface oxygen loss and subsequent transition metal reduction. Particularly at 4.75 V, thermal aggravation further enhances active material degradation, which results in substantial transition metal dissolution and subsequent plating at the lithium anode.[22] Possible reaction mechanisms that promote surface oxygen loss as a result of carbonate solvent and salt breakdown are further discussed in a previous paper.[22]

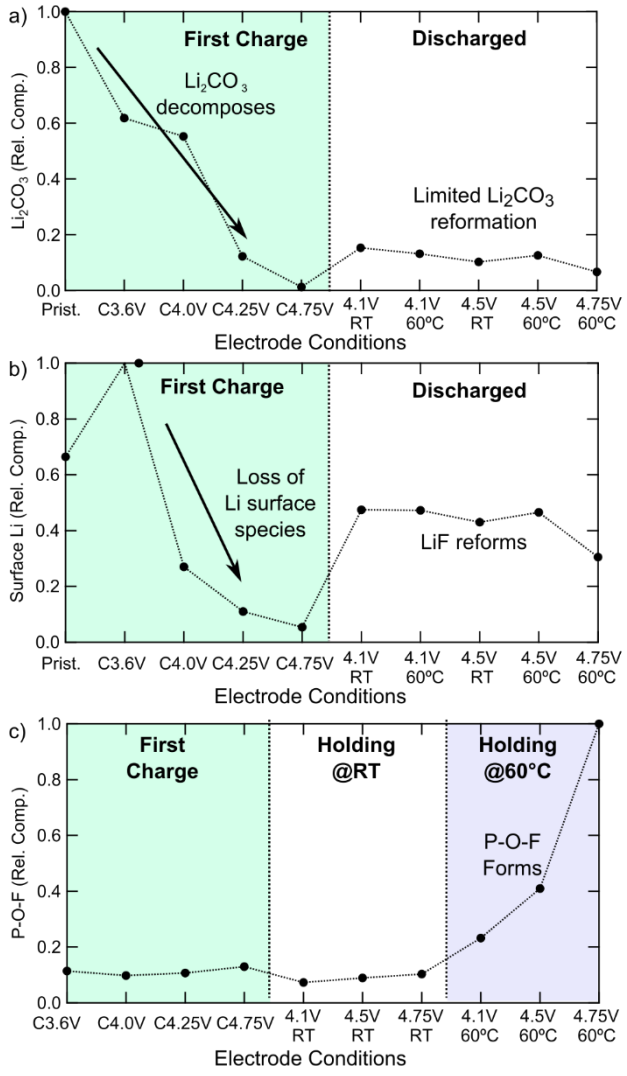

Figure 12. Relative compositions of the a) Li_2CO_3, b) Li surface species, and c) P-O-F surface species based on fitting of the O K-edge, Li 1s and P 2p core region respectively for SOC electrodes and held electrodes measured in the discharged state. These electrodes were held for two weeks except for the 4.75 V and 60°C electrode which was held for 10 hours.

Finally, the evolution of LiF during charge and discharge warrants further study. Unlike Li_2CO_3, discharging to 2.7 V resulted in LiF at the CEI with the quantity dependent on the holding voltage and temperature as shown in Fig. 12b. A similar evolution of LiF has been reported on the graphite surface within a $LiCoO_2$/graphite full cell when the cell potential was between 3.8V and 4.2V during the first and fifth cycle.[4] More work is needed to understand the formation and stability of LiF at both EEIs.

CONCLUSION

This study has revealed a strong temperature dependence of the $LiPF_6$ breakdown which drives degradation of the cathode surface. We have further ruled out the influence of Li_2CO_3 or other lithium species (LiF) on impedance growth at the cathode surface at high voltages. It is interesting to note that LiF is observed to reform on the surface while Li_2CO_3 does not after electrodes are discharged to 2.7 V.

By holding NCA electrodes at high voltages, we correlate $LiPF_6$ breakdown with active material degradation. We highlight the importance of the stability of the electrolyte salt at high voltages and high temperatures. $LiPF_6$ seems relatively stable at RT yet undergoes marked breakdown at 60°C that promotes transition metal reduction. More work is needed to select additives or salts with higher thermal stability to utilize the higher capacities obtainable with nearly full delithiation of NCA.

ASSOCIATED CONTENT

Supporting Information. Additional x-ray spectroscopy measurements are shown in supplementary related to reproducibility, loss of Li_2CO_3, trace electrolyte decomposition for electrodes held at room temperature and bulk sensitive TFY measurements.

AUTHOR INFORMATION

Corresponding Author

* Email: lpiper@binghamton.edu (L. F. J. Piper)

ACKNOWLEDGMENT

This work was supported as part of NECCES, an Energy Frontier Research Center funded by the U.S. Department of Energy, Office of Science, Office of Basic Energy Sciences under Award No. DE-SC0012583. XAS experiments were performed at beamline 8.0.1 at the ALS and beamline I09 at Diamond Light Source. The work at ALS was supported by the Office of Basic Energy Sciences, of the U.S. Department of Energy under Contract No. DE-AC02-05CH11231. Z. W. L.-H. and S. S. gratefully acknowledges support from a Doctoral Fellowship in Residence Award from the ALS. We thank Diamond Light Source for access to beamline I09 (SI12764 & SI16005) that contributed to the results presented here. D.M.H. is grateful to Dr. Ieuan Seymour, Dr. Gunwoo Kim, and Philip Reeves for useful discussions, suggestions, and experimental assistance.

REFERENCES

(1) Xu, K. Nonaqueous Liquid Electrolytes for Lithium-Based Rechargeable Batteries. *Chem. Rev.* **2004**, *104*, 4303–4417.

(2) Gauthier, M.; Carney, T. J.; Grimaud, A.; Giordano, L.; Pour, N.; Chang, H.-H.; Fenning, D. P.; Lux, S. F.; Paschos, O.; Bauer, C.; Maglia, F.; Lupart, S.; Lamp, P.; Shao-Horn, Y. The Electrode-

Electrolyte Interface in Li-Ion Batteries: Current Understanding and New Insights. *J. Phys. Chem. Lett.* **2015**, *6*, 4653-4672

(3) Aurbach, D.; Markovsky, B.; Shechter, A.; Ein-Eli, Y.; Cohen, H. A Comparative Study of Synthetic Graphite and Li Electrodes in Electrolyte Solutions Based on Ethylene Carbonate-Dimethyl Carbonate Mixtures. *J. Electrochem. Soc.* **1996**, *143*, 3809–3820.

(4) Leroy, S.; Blanchard, F.; Dedryvère, R.; Martinez, H.; Carré, B.; Lemordant, D.; Gonbeau, D. Surface Film Formation on a Graphite Electrode in Li-Ion Batteries: AFM and XPS Study. *Surf. Interface Anal.* **2005**, *37*, 773–781.

(5) Fong, R; von Sacken, U.; Dahn, J. R. Studies of Lithium Intercalation in Carbons Using Nonaqueous Electrochemical Cells. **1990**, *137*, 2009-2013.

(6) Amatucci, G.; Tarascon, J. M.; Klein, L. C. Cobalt Dissolution in $LiCoO_2$-Based Non-Aqueous Rechargeable Batteries. *Solid State Ionics* **1996**, *83*, 167–173.

(7) Lin, F.; Markus, I. M.; Nordlund, D.; Weng, T.-C.; Asta, M. D.; Xin, H. L.; Doeff, M. M. Surface Reconstruction and Chemical Evolution of Stoichiometric Layered Cathode Materials for Lithium-Ion Batteries. *Nat. Commun.* **2014**, *5*, 3529.

(8) Ma, L.; Xia, J.; Dahn, J. R. Improving the High Voltage Cycling of $Li[Ni_{0.42}Mn_{0.42}Co_{0.16}]O_2$ (NMC442)/Graphite Pouch Cells Using Electrolyte Additives. *J. Electrochem. Soc.* **2014**, *161*, A2250–A2254.

(9) Sallis, S.; Pereira, N.; Mukherjee, P.; Quackenbush, N. F.; Faenxza, N.; Schlueter, C.; Lee, T. L.; Yang, W. L.; Cosandey, F.; Amatucci, G. G.; Piper, L. F. J. Surface Degradation of $Li_{1-x}Ni_{0.80}Co_{0.15}Al_{0.05}O_2$ Cathodes: Correlating Charge Transfer Impedance with Surface Phase Transformations. *Appl. Phys. Lett.* **2016**, *108*, 1–5.

(10) Zhang, Y.; Wang, C.-Y. Cycle-Life Characterization of Automotive Lithium-Ion Batteries with $LiNiO_2$ Cathode. *J. Electrochem. Soc.* **2009**, *156*, A527-A535.

(11) Kim, H.-G.; Myung, S.-T.; Lee, J. K.; Sun, Y.-K. Effects of Manganese and Cobalt on the Electrochemical and Thermal Properties of Layered $Li[Ni_{0.52}Co_{0.16+x}Mn_{0.32-x}]O2$ Cathode Materials. *J. Power Sources* **2011**, *196*, 6710–6715.

(12) Andersson, a. M.; Abraham, D. P.; Haasch, R.; MacLaren, S.; Liu, J.; Amine, K. Surface Characterization of Electrodes from High Power Lithium-Ion Batteries. *J. Electrochem. Soc.* **2002**, *149*, A1358-A1369.

(13) Shikano, M.; Kobayashi, H.; Koike, S.; Sakaebe, H.; Ikenaga, E.; Kobayashi, K.; Tatsumi, K. Investigation of Positive Electrodes after Cycle Testing of High-Power Li-Ion Battery Cells II. An Approach to the Power Fading Mechanism Using Hard X-Ray Photoemission Spectroscopy. *J. Power Sources* **2007**, *174*, 795–799.

(14) Abraham, D. P.; Twesten, R. D.; Balasubramanian, M.; Kropf, J.; Fischer, D.; McBreen, J.; Petrov, I.; Amine, K. Microscopy and Spectroscopy of Lithium Nickel Oxide-Based Particles Used in High Power Lithium-Ion Cells. *J. Electrochem. Soc.* **2003**, *150*, A1450-A1456.

(15) Hwang, S.; Kim, S. M.; Bak, S. M.; Cho, B. W.; Chung, K. Y.; Lee, J. Y.; Chang, W.; Stach, E. A. Investigating Local Degradation and Thermal Stability of Charged Nickel-Based Cathode Materials through Real-Time Electron Microscopy. *ACS Appl. Mater. Interfaces* **2014**, *6*, 15140–15147.

(16) Verdier, S.; El Ouatani, L.; Dedryvère, R.; Bonhomme, F.; Biensan, P.; Gonbeau, D. XPS Study on Al_2O_3- and $AlPO_4$-Coated $LiCoO_2$ Cathode Material for High-Capacity Li Ion Batteries. *J. Electrochem. Soc.* **2007**, *154*, A1088-A1099.

(17) Tebbe, J. L.; Holder, A. M.; Musgrave, C. B. Mechanisms of $LiCoO_2$ Cathode Degradation by Reaction with HF and Protection by Thin Oxide Coatings. *ACS Appl. Mater. Interfaces* **2015**, *7*, 24265–24278.

(18) Eriksson, T.; Andersson, A. M.; Bishop, A. G.; Gejke, C.; Gustafsson, T.; Thomas, J. O. Surface Analysis of $LiMn_2O_4$ Electrodes in Carbonate-Based Electrolytes. *J. Electrochem. Soc.* **2002**, *149*, A69-A78.

(19) Edström, K.; Gustafsson, T.; Thomas, J. O. The Cathode – Electrolyte Interface in the Li-Ion Battery. *Electrochemica Acta* **2004**, *50*, 397–403.

(20) Pieczonka, N. P. W.; Liu, Z.; Lu, P.; Olson, K. L.; Moote, J.; Powell, B. R.; Kim, J.-H. Understanding Transition-Metal Dissolution Behavior in $LiNi_{0.5}Mn_{1.5}O_4$ High-Voltage Spinel for Lithium Ion Batteries. *J. Phys. Chem. C* **2013**, *117*, 15947–15957.

(21) Quinlan, R. A.; Lu, Y.-C.; Shao-Horn, Y.; Mansour, A. N. XPS Studies of Surface Chemistry Changes of $LiNi_{0.5}Mn_{0.5}O_2$ Electrodes during High-Voltage Cycling. *J. Electrochem. Soc.* **2013**, *160*, A669–A677.

(22) Faenza, N. V; Lebens-higgins, Z. W.; Mukherjee, P.; Sallis, S.; Pereira, N.; Badway, F.; Halajko, A.; Ceder, G.; Cosandey, F.; Piper, L. F. J.; Amatucci, G. G. Electrolyte Induced Surface Transformation and Transition Metal Dissolution of Fully Delithiated Layered Compounds. *Langmuir* **2017**. *33*, 9333–9353

(23) Markevich, E.; Salitra, G.; Aurbach, D. Influence of the PVdF Binder on the Stability of $LiCoO_2$ Electrodes. *Electrochem. commun.* **2005**, *7*, 1298–1304.

(24) Watanabe, S.; Kinoshita, M.; Hosokawa, T.; Morigaki, K.; Nakura, K. Capacity Fade of $LiAl_yNi_{1-x-y}Co_xO_2$ Cathode for Lithium-Ion Batteries during Accelerated Calendar and Cycle Life Tests (Surface Analysis of $LiAl_yNi_{1-x-y}Co_xO_2$ Cathode after Cycle Tests in Restricted Depth of Discharge Ranges). *J. Power Sources* **2014**, *258*, 210–217.

(25) Dallera, C.; Duò, L.; Braicovich, L.; Panaccione, G.; Paolicelli, G.; Cowie, B.; Zegenhagen, J. Looking 100 Å Deep into Spatially Inhomogeneous Dilute Systems with Hard X-Ray Photoemission. *Appl. Phys. Lett.* **2004**, *85*, 4532–4534.

(26) Lu, Y. C.; Mansour, A. N.; Yabuuchi, N.; Shao-Horn, Y. Probing the Origin of Enhanced Stability of $AlPO_4$ Nanoparticle Coated $LiCoO_2$ during Cycling to High Voltages: Combined XRD and XPS Studies. *Chem. Mater.* **2009**, *21*, 4408–4424.

(27) Zuo, X.; Fan, C.; Liu, J.; Xiao, X.; Wu, J.; Nan, J. Lithium Tetrafluoroborate as an Electrolyte Additive to Improve the High Voltage Performance of Lithium-Ion Battery. **2013**, *160*, 1199–1204.

(28) Baggetto, L.; Dudney, N. J.; Veith, G. M. Surface Chemistry of Metal Oxide Coated Lithium Manganese Nickel Oxide Thin Film Cathodes Studied by XPS. *Electrochim. Acta* **2013**, *90*, 135–147.

(29) de Groot, F. M. F. X-Ray Absorption Spectroscopy and Dichroism of Transition Metals and Their Compounds. *J. Electron Spectros. Relat. Phenomena* **1994**, *67*, 529–622.

(30) Yoon, W. S.; Chung, K. Y.; McBreen, J.; Fischer, D. A.; Yang, X. Q. Electronic Structural Changes of the Electrochemically Li-Ion Deintercalated $LiNi_{0.8}Co_{0.15}Al_{0.05}O_2$ Cathode Material Investigated by X-Ray Absorption Spectroscopy. *J. Power Sources* **2007**, *174*, 1015–1020.

(31) Qiao, R.; Chuang, Y. De; Yan, S.; Yang, W. Soft X-Ray Irradiation Effects of Li_2O_2, Li_2CO_3 and Li_2O Revealed by Absorption Spectroscopy. *PLoS One* **2012**, *7*, 3–8.

(32) Robert, R.; Bunzli, C.; Berg, E. J.; Novák, P. Activation Mechanism of $LiNi_{0.80}Co_{0.15}Al_{0.05}O_2$: Surface and Bulk Operando Electrochemical, Differential Electrochemical Mass Spectrometry, and X-Ray Diffraction Analyses. *Chem. Mater.* **2015**, *27*, 526–536.

(33) Niu, K.; Lin, F.; Fang, L.; Nordlund, D.; Tao, R.; Weng, T. Structural and Chemical Evolution of Amorphous Nickel Iron Complex Hydroxide upon Lithiation/Delithiation. *Chem. Mater.* **2015**. 27, 1583-1589

(34) Shkrob, I. A.; Gilbert, J. A.; Phillips, P. J.; Klie, R.; Haasch, R. T.; Bareño, J.; Abraham, D. P. Chemical Weathering of Layered Ni-Rich Oxide Electrode Materials: Evidence for Cation Exchange. *J. Electrochem. Soc.* **2017**, *164*, A1489–A1498.

(35) Bi, Y.; Wang, T.; Liu, M.; Du, R.; Yang, W.; Liu, Z.; Peng, Z.; Liu, Y.; Wang, D.; Sun, X. Stability of Li_2CO_3 in Cathode of Lithium Ion Battery and Its Influence on Electrochemical Performance. *RSC Adv.* **2016**, *6*, 19233–19237.

(36) Yang, S.; Wang, D.; Liang, G.; Yiu, Y. M.; Wang, J.; Liu, L.; Sun, X.; Sham, T.-K. Soft X-Ray XANES Studies of Various Phases Related to $LiFePO_4$ Based Cathode Materials. *Energy Environ. Sci.* **2012**, *5*, 7007-7016.

(37) Campion, C. L.; Li, W.; Lucht, B. L. Thermal Decomposition of $LiPF_6$-Based Electrolytes for Lithium-Ion Batteries. *J. Electrochem. Soc.* **2005**, *152*, A2327-A2334.

(38) In the work of Campion *et al.*, the ^{19}F shifts have been referenced to $LiPF_6$ at 65 ppm, which is a non-standard shift

scale; here, we reference the ^{19}F shifts to PTFE at -123 ppm, and have recalculated the previously reported shifts accordingly, which differ by +140 ppm.

(39) Biesinger, M. C.; Payne, B. P.; Grosvenor, A. P.; Lau, L. W. M.; Gerson, A. R.; Smart, R. S. C. Resolving Surface Chemical States in XPS Analysis of First Row Transition Metals, Oxides and Hydroxides: Cr, Mn, Fe, Co and Ni. *Appl. Surf. Sci.* **2011**, *257*, 2717–2730.

(40) Markevich, E.; Salitra, G.; Fridman, K.; Sharabi, R.; Gershinsky, G.; Garsuch, A.; Semrau, G.; Schmidt, M. A.; Aurbach, D. Fluoroethylene Carbonate as an Important Component in Electrolyte Solutions for High-Voltage Lithium Batteries: Role of Surface Chemistry on the Cathode. *Langmuir* **2014**, *30*, 7414–7424.

(41) Duncan, H.; Duguay, D.; Abu-lebdeh, Y.; Davidson, I. J. Study of the $LiMn_{1.5}Ni_{0.5}O_4$/Electrolyte Interface at Room Temperature and 60°C. *J. Electrochem. Soc.* **2011**, *158*, 537–545.

(42) Cho, D.-H.; Jo, C.-H.; Cho, W.; Kim, Y.-J.; Yashiro, H.; Sun, Y.-K.; Myung, S.-T. Effect of Residual Lithium Compounds on Layer Ni-Rich $Li[Ni_{0.7}Mn_{0.3}]O_2$. *J. Electrochem. Soc.* **2014**, *161*, A920–A926.

(43) Tasaki, K.; Goldberg, A.; Lian, J.-J.; Walker, M.; Timmons, A.; Harris, S. J. Solubility of Lithium Salts Formed on the Lithium-Ion Battery Negative Electrode Surface in Organic Solvents. *J. Electrochem. Soc.* **2009**, *156*, A1019-A1027.

(44) Grenier, A.; Liu, H.; Wiaderek, K. M.; Lebens-Higgins, Z. W.; Borkiewicz, O. J.; Piper, L. F. J.; Chupas, P. J.; Chapman, K. W. Reaction Heterogeneity in $LiNi_{0.8}Co_{0.15}Al_{0.05}O_2$ Induced by Surface Layer. *Chem. Mater.* **2017**, 29 7345-7352